2024 IEEE International Conference on Robotics and Automation (ICRA 2024)
May 13-17, 2024. Yokohama, Japan

Rolling with Planar Parametric Curves for Real-time Robot Locomotion Algorithms

Adwait Mane and Christian Hubicki

***Abstract*— Robots routinely encounter obstacles and rough terrain, but terrain curvature is seldom included in models for real-time algorithms. We present a closed-form dynamic model for rolling with two planar smooth curves, and apply it to sagittal-plane locomotion problems. We assumed that the body rolls without slip and maintains a single point of contact. Using an auxiliary coordinate system to define the rolling body and terrain as parametric curves, we derived rolling constraints and dynamic equations of motion for model-based control algorithms – specifically Operational Space Control. The formulation was used to simulate an arbitrarily curved rock rolling on undulating terrain and to generate control signals to stabilize it on parabolic terrain. The stabilization problem was solved as a quadratic program in < 3 ms which shows that our formulation is suitable for real-time control algorithms. We also applied this framework to dynamically balance an underactuated 2 degree-of-freedom leg on parabolic terrain and achieve prescribed locomotion tasks for a wheel-leg vehicle on sinusoidal terrain in simulation. A supplementary video is available at https://youtu.be/EtPQEzkqsK8.**

I. Introduction

Rough terrain locomotion has been a long-standing challenge in robotics. Robots with wheels [1][2], tracks, legs, and combinations thereof [3][4][5][6] have been developed to tackle this challenge. In general, the terrain geometry is nonlinear in such scenarios. Moderate roughness can be treated as a disturbance on nominally linear terrain, but awareness of terrain curvature is necessary for nonlinear ground profiles (Fig. 1). Closed-form models can enable real-time model-based planning, control, and estimation [7][8], but model-based methods have rarely been applied to rolling on curves in robotic locomotion. We present a closed-form dynamic model for planar no-slip rolling between two smooth parametric curves, assuming a single contact point. We then apply this model to real-time robot locomotion control on curved terrain in simulation.

Rolling on curves is a common phenomenon in locomotion (Fig. 1). It occurs when wheeled or tracked robots drive over curved obstacles or valleys. In legged locomotion, the foot geometry can influence gait [9]. Legged robots are often modeled with point [10][11][12] or flat feet, and sometimes curved feet [13][14]. Both flat and curve-footed robots can exhibit rolling behavior while traversing curved obstacles.

*This work was supported by L3Harris Technologies, Inc. and the Toyota Research Institute.

The authors are with the Department of Mechanical Engineering, FAMU-FSU College of Engineering, Florida State University, Tallahassee, FL 32310, USA. Corresponding author: Adwait Mane, am19db@fsu.edu

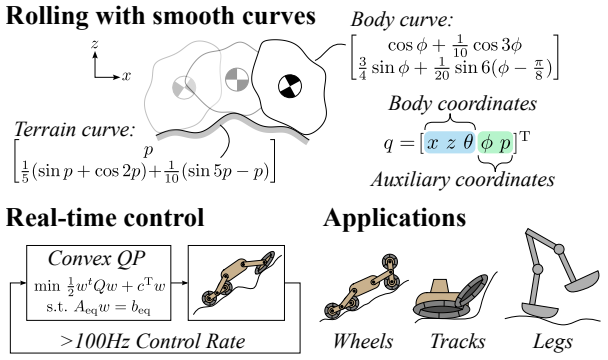

Fig. 1 **Overview.** Rolling on curves occurs in a variety of locomotion scenarios. Our closed-form model for no-slip rolling is computationally tractable for real-time control.

A. Literature review

The governing equations for a circular wheel rolling on linear terrain are widely known. Rolling on curved terrain is more challenging than appears at first glance. This is illustrated by the coin rolling paradox [15], which shows that the arc length traversed depends on the curvature of the terrain (Section II-B).

The kinematics of rolling on curves has been studied in the context of roulette curves. A roulette curve is the locus of a point fixed to a moving curve as it rolls without slipping on a stationary curve [16][17]. It is a generalization of the cycloid - the solution to the famous *brachistochrone* problem [18]. However, closed-form solutions have only been found for specific instances of stationary and moving curves. Moreover, roulette curves are not parameterized in the terms of rotation angle, which makes them impractical for deriving rolling kinematics and dynamics.

Rolling on curves has been studied for mechanism design [19][20][21]. It has also been studied in the context of robotic manipulation [22][23][24][25][26]. Some of these studies assume the presence of tactile sensors to locate the contact point [22][23]; however, these sensors are less likely to be present in locomotion systems. Others consider special cases of constant curvature geometries [20][21][24][25]. Woodruff and Lynch's formulation [26] applies to non-constant curvatures but assumes an orthogonal surface parameterization, limiting its applicability to ellipses and ellipsoids. In contrast, our approach extends to more intricate planar geometries, provided that the single-contact-point assumption holds.

Techniques for simulation of rigid bodies through contact

have been developed in the computer graphics and applied mechanics communities [27][28][29]. Irregular geometries are represented using a mesh. A mesh-based simulation framework requires collision detection and a contact force solver [27] even for single-contact-point rolling. These componets can be computationally expensive. Our focus and approach is different, so we do not require these additional components. There is no need for collision detection since we consider continuous contact, and contact forces are included as Lagrange multipliers in our augmented dynamics formulation. For continuous contact, complementarity and penalty-based are two common approaches to simulation [29]. Linear complementarity problems (LCPs) are nonlinear[1] and potentially non-convex ([7] appendix B, [28][30]). Anitescu developed a convex relaxation for LCPs [31] but this is difficult to implement in practice for rolling contact [32] and computational complexity remains a practical challenge ([33] section 4.10). Applying the complementarity framework for real-time robotic applications is an active research area [34][35]. Overall, our approach to modeling rolling contact is computationally simpler.

Curved feet play an important role in legged locomotion. When humans walk, the center of pressure shifts forward from heel to toe during each step. Adamczyk *et al.* reported that the ankle, foot, and shoe interact to produce a movement similar to that of a rigid curved foot [36]. They performed experiments on human subjects where rigid circular arcs were attached under the subjects' boots. They tested various foot radii and found that a foot radius to leg length ratio of 0.3 minimized the metabolic cost of walking. This has inspired the development of bipedal robots with curved feet which achieve greater energy efficiency compared to point or flat feet [37][38].

Several other studies have used curved feet for model-based bipedal robot locomotion. Martin *et al.* designed a controller based on virtual constraints and hybrid zero dynamics for a planar biped with circular feet [39]. They found that a closed-form expression determines the existence of a periodic orbit, and hardware experiments showed lower cost of transport and joint tracking errors for the circular foot gaits. Curved feet are also prominent in the passive dynamics paradigm, which has produced human-like gait dynamics on the most energy-efficient walking robots. McGeer's pioneering planar passive dynamic walker [40] and the minimally actuated Cornell Ranger [14] had circular feet. Collins *et al.* developed a three-dimensional passive dynamic walker with specially designed elliptical feet [41]. All of these studies assumed circular feet (except [41]) and linear terrain. Our model is general enough to represent both the foot and the terrain using any smooth parametric curve. A curved terrain model can be helpful for model-based control on rough terrain and obstacles.

[1]LCPs are called linear because one of the constraints is linear, but the complementarity constraint is nonlinear ([28] section 1.4).

B. Contributions

We previously developed a motion planning framework for planar wheel-leg and track-leg Unmanned Ground Vehicles (UGVs) with intermittent contact on piecewise linear terrain [42]. In the previous work, we considered circular and elliptical body geometries. In this work we extended the previous framework and developed a closed-form model for two smooth, planar parametric curves to roll without slip, assuming a single contact point. We also developed a model-based Operational Space Controller to achieve objectives defined in the task space via feedback control.

II. Methods

Here we describe our closed-form dynamic model and control strategy for rolling with two smooth parametric curves. We start with the simple cases of a wheel on linear and circular terrain to illustrate the difficulty of deriving rolling kinematics for curved terrain. Next, we introduce an auxiliary formulation which provides a practical alternative. Finally, we describe our dynamics formulation and control algorithm.

For notation, scalars are italic (x, y, L), and vectors and matrices are bold and upright ($\mathbf{q}$, $\boldsymbol{\lambda}$, $\mathbf{A}$). We now state the arc length formulae used. For an explicit curve $z = f(x)$, the arc length is

$$s = \int_a^b \sqrt{1 + \left(\frac{\mathrm{d}z(x)}{\mathrm{d}x}\right)^2} \ \mathrm{d}x \ , \tag{1}$$

and for a parametric curve $\begin{bmatrix} x & z \end{bmatrix}^\top = \alpha(p)$, the arc length is

$$s = \int_a^b \left\| \frac{\mathrm{d}\alpha(p)}{\mathrm{d}p} \right\|_2 \ \mathrm{d}p \ . \tag{2}$$

A. Rolling on linear terrain

We present the constraints for rolling without slip on linear terrain $z_{ter}(x) = mx_{ter} + c$, where $m = \tan\psi$ and c are scalar constants. The coordinates $\mathbf{q} = \begin{bmatrix} x & z & \theta \end{bmatrix}_{wh}^\top$ represent the center position and orientation of an unconstrained wheel with radius r_{wh}.

On linear terrain, the arc length traversed by a wheel is

$$s_{wh} = r_{wh}\theta_{wh}. \tag{3}$$

From (1), the arc length traversed along the terrain is the Euclidean distance,

$$s_{ter} = \sqrt{\Delta x_{ter}^2 + \Delta z_{ter}^2} = \sqrt{\Delta x_{wh}^2 + \Delta z_{wh}^2}. \tag{4}$$

For no-slip rolling, $s_{wh} = s_{ter}$. Therefore, the arc length constraint is

$$h_1(\mathbf{q}) = \sqrt{\Delta x_{wh}^2 + \Delta z_{wh}^2} - r_{wh}\Delta\theta_{wh} = 0. \tag{5}$$

Since the wheel center follows a path parallel to the terrain, the center position constraint is

$$h_2(\mathbf{q}) = z_{wh} - mx_{wh} - (c + r_{wh}/\cos\psi) = 0. \tag{6}$$

The three coordinates $\mathbf{q} = \begin{bmatrix} x & z & \theta \end{bmatrix}_{wh}^\top$ and the two constraints (5) and (6) define the kinematics for a 1 degree of freedom (DoF) system that rolls without slip.

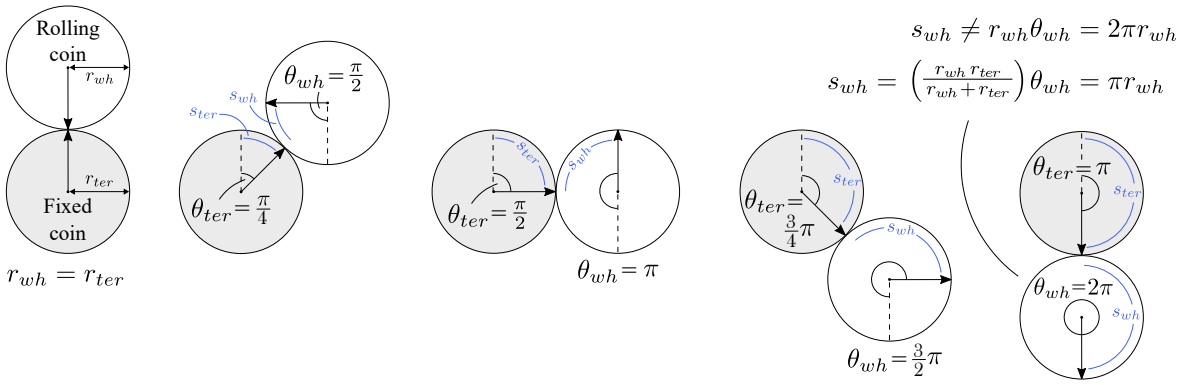

Fig. 2 **Coin rolling paradox.** This example shows that the arc length traversed depends both on the wheel rotation (θ_{wh}) and the terrain curvature.

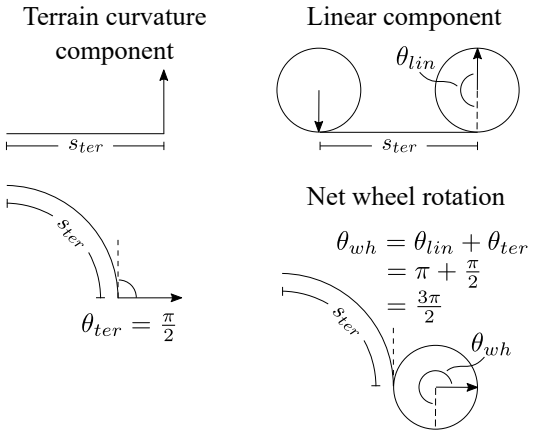

Fig. 3 **Components of rotation on curved terrain.** The net wheel rotation (θ_{wh}) is the sum of the linear component (θ_{lin}) and the rotation due to the terrain curvature (θ_{ter}), but only (θ_{lin}) contributes to the arc length traversed.

B. Circular terrain: coin rolling paradox

The kinematics of rolling on curved terrain are fundamentally different. This is illustrated by the coin rolling paradox[2] [15]. Consider a circular coin rolling without slip on a fixed coin of the same radius. If the wheel rotation θ_{wh} is 2π rad, what is the arc length, s_{wh}, traversed by the wheel? The intuitive response, based on (3), is $s_{wh} = r_{wh}\theta_{wh} = 2\pi r_{wh}$. However, this is incorrect. As seen in Fig. 2 and in the supplementary video, the correct answer is $s_{wh} = \pi r_{wh}$. We encourage the reader to try this simple experiment with two coins.

Fig. 3 provides intuition for why $s_{wh} \neq r_{wh}\theta_{wh}$ for curved terrain. Rolling on curved terrain consists of two components,

$$\theta_{wh} = \theta_{lin} + \theta_{ter}, \tag{7}$$

where θ_{lin} is the *linear* component. We call it *linear* because this is the wheel rotation required to traverse an equivalent arc length on linear terrain. θ_{ter} is the wheel rotation due to the curvature of the terrain.

[2]The coin rolling paradox was in the news when it appeared on an SAT exam and the examiners arrived at the incorrect answer [43].

Remark 1. *For a circular wheel rolling without slip on curved terrain, only the linear component (θ_{lin}) of the net wheel rotation (θ_{wh}) contributes to the arc length traversed (s_{wh}) (Fig. 3).*

Therefore, the correct formula for no-slip rolling on curved terrain is

$$s_{wh} = r_{wh}\theta_{lin}. \tag{8}$$

In our coin rolling example, $\theta_{wh} = 2\pi$ rad, and $\theta_{lin} = \theta_{ter} = \pi$ rad. Applying (8) gives the correct answer $s_{wh} = \pi r_{wh}$ (Fig. 2).

Since θ_{wh} is a coordinate in $\mathbf{q}$, but θ_{lin} is not, it is more useful to derive $s_{wh} = f(\theta_{wh})$. For circular terrain,

$$s_{ter} = r_{ter}\theta_{ter}. \tag{9}$$

Using the no-slip condition $s_{wh} = s_{ter}$ and substituting (8) and (9) into (7), we get

$$s_{wh} = \left(\frac{r_{wh}r_{ter}}{r_{wh}+r_{ter}}\right)\theta_{wh} \tag{10}$$

for a circular wheel rolling without slip on circular terrain.

Remark 2. *For a circular wheel rolling without slip on curved terrain, the arc length traversed depends on the wheel rotation (θ_{wh}) as well as the curvature of the terrain.*

We now write the rolling constraints for this problem. It is difficult to derive an arc length constraint analogous to (5), but we can use an alternate form. From $z_{wh} = R\cos(\theta_{ter})$, where $R = r_{ter} + r_{wh}$, we get

$$h_1(\mathbf{q}) = z_{wh} - R\cos\left(\left(\frac{r_{wh}}{r_{wh}+r_{ter}}\right)\theta_{wh}\right). \tag{11}$$

The wheel center path constraint is

$$h_2(\mathbf{q}) = x_{wh}^2 + z_{wh}^2 - R^2 = 0, \tag{12}$$

analogous to (6). Note that these constraint expressions are non-unique so other formulations also exist.

C. Challenges for arbitrary curves

We now consider the case where the rolling body and the terrain have variable curvature (Fig. 1). We need to derive constraint expressions in the form $h(\mathbf{q}) = 0$. We were able to do this for the case of a circular body rolling on constant curvature (linear and circular) terrain using the coordinates

$\mathbf{q} = \begin{bmatrix} x & z & \theta \end{bmatrix}^\top_{wh}$ for the rolling body. For the general case, (3) and (10) take the general form $s_{bod} = f(\kappa_{bod}, \kappa_{ter}, \theta_{bod})$ where κ_{bod} and κ_{ter} are the curvatures of the rolling body and terrain, both of which vary along the curves. While it may be theoretically possible to find closed-form expressions for s_{bod} and $h(\mathbf{q})$ for the general case, we found this difficult in practice. Therefore, we developed an auxiliary formulation as a tractable alternative.

D. Auxiliary formulation

We used three coordinates and two constraints for the linear and circular terrain cases. The kinematic of rolling between variable curvature curves are easier to derive using five coordinates and four constraints [44]. We introduce the auxiliary coordinates ϕ and p and define the coordinate vector $\mathbf{q} = \begin{bmatrix} x & z & \theta & \phi & p \end{bmatrix}^\top$. ϕ and p are the parameters for the curves $\boldsymbol{\alpha}_{bod}(\phi)$ and $\boldsymbol{\alpha}_{ter}(p)$ for the rolling body and the terrain. $\boldsymbol{\alpha}_{ter}(p)$ is defined in the global frame and $\boldsymbol{\alpha}_{bod}(\phi)$ is defined in the body-fixed frame (Fig. 4). $\mathbf{T}_{ter}$ and $\mathbf{T}_{bod}$ are the unit tangent vectors. We assume that the parametric curves $\boldsymbol{\alpha}_{bod}(\phi)$ and $\boldsymbol{\alpha}_{ter}(p)$ are smooth. They can have convex and concave regions as long as a single point of contact is maintained during rolling.

The general governing principles for rolling without slip between two smooth curves are (Fig. 5) [42]:

1) The arc lengths traversed along the two curves by the contact points are equal.
2) The tangent vectors at the contact points on both curves are aligned.
3) The two curves remain in contact at all times *i.e.* no penetration or separation.

The arc length integral (2) may not have a closed form solution for some curves, such as ellipses, so we derived an expression for the time derivative of (2) and implemented the constraints in velocity form:

$$\frac{\mathrm{d}\mathbf{h}(\mathbf{q})}{\mathrm{d}t} = \begin{bmatrix} \|\boldsymbol{\alpha}'_{bod}(\phi)\|_2 \ \dot{\phi} + \|\boldsymbol{\alpha}'_{ter}(p)\|_2 \dot{p} \\ \frac{\mathrm{d}}{\mathrm{d}t}\left(\mathbf{R}(\theta)\mathbf{T}_{bod}(\phi) \cdot \mathbf{T}_{ter}(p)\right) \\ \frac{\mathrm{d}}{\mathrm{d}t}\Big(\begin{bmatrix} x & z \end{bmatrix}^\top - \boldsymbol{\alpha}_{ter}(p) + \mathbf{R}(\theta)\boldsymbol{\alpha}_{bod}(\phi)\Big) \end{bmatrix} = 0 \quad (13)$$

where $\mathbf{R}(\theta)$ is the rotation matrix from the body-fixed frame to the global frame. The first two are scalar equations for the arc length and tangent constraints, and the third is a vector equation for the path of the body center.

E. Augmented dynamics formulation

The dynamic equations of motion were derived using Lagrange's equations with holonomic constraints [45],

$$\frac{\mathrm{d}}{\mathrm{d}t}\left(\frac{\partial L}{\partial \dot{\mathbf{q}}}\right)^\top - \left(\frac{\partial L}{\partial \mathbf{q}}\right)^\top = \mathbf{u} + \boldsymbol{\Gamma}, \quad (14)$$

where t is time, $\mathbf{q}$ and $\dot{\mathbf{q}}$ are the position and velocity, L and $\mathbf{u}$ are the Lagrangian and the actuator input. $\boldsymbol{\Gamma} = \mathbf{A}(\mathbf{q})^\top \boldsymbol{\lambda}$ represents the forces for the constraints $\mathbf{h}(\mathbf{q})$, where $\mathbf{A}(\mathbf{q}) = \partial \mathbf{h}(\mathbf{q}) / \partial \mathbf{q}$ is the constraint Jacobian and $\boldsymbol{\lambda}$ are the Lagrange multipliers.

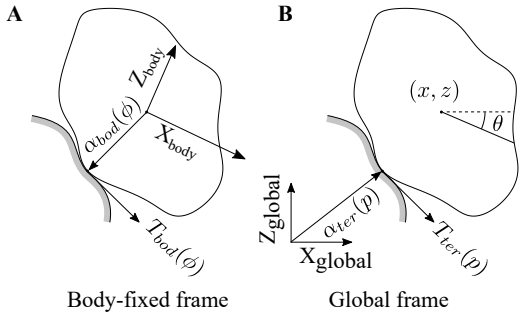

Fig. 4 **Parametric curves for the rolling body and the terrain.** The body-fixed frame (X_{body}, Z_{body}) moves with the rolling body.

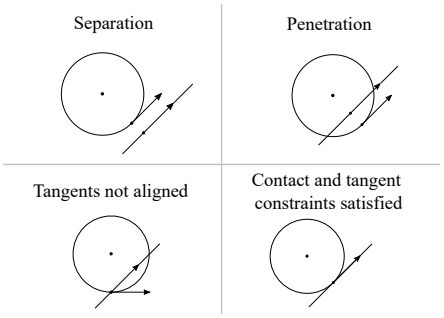

Fig. 5 **Contact and tangent constraints for rolling [42].** These constraints need to be satisfied for correct rolling behavior.

We take the time derivative of (13) to get $\mathrm{d}^2\mathbf{h}(\mathbf{q})/\mathrm{d}t^2$. This can be written in an augmented form with the second-order dynamic equations (14) to obtain a set of index-1 Differential-Algebraic Equations (DAEs) [44]:

$$\widehat{\mathbf{M}}\,\ddot{\widehat{\mathbf{q}}} = \widehat{\mathbf{f}} + \widehat{\mathbf{u}} \ \Rightarrow \begin{bmatrix} \mathbf{M} & -\mathbf{A}^\top \\ \mathbf{A} & \mathbf{0} \end{bmatrix} \begin{bmatrix} \ddot{\mathbf{q}} \\ \boldsymbol{\lambda} \end{bmatrix} = \begin{bmatrix} \mathbf{G} \\ \mathbf{H} \end{bmatrix} + \widehat{\mathbf{u}}, \quad (15)$$

$\widehat{\mathbf{M}}$ and $\ddot{\widehat{\mathbf{q}}}$ are the augmented inertia and acceleration. We need to solve for $\ddot{\widehat{\mathbf{q}}}$ to simulate the system but $\widehat{\mathbf{M}}$ is not invertible for the auxiliary formulation. This is because the constraints (13) are redundant. However, a solution does exist for this system since any possible movement involves a positive kinetic energy [46].

F. Model-based Operational Space Controller (OSC)

We used an OSC [47] to achieve desired task space dynamics. $\ddot{\mathbf{x}}$ and $\ddot{\mathbf{x}}_{des}$ are the current and desired task space accelerations. $\ddot{\mathbf{x}}_{des}$ is computed using a PD control law. The optimization is formulated as

$$\begin{aligned} \min_{\ddot{\widehat{\mathbf{q}}}, \widehat{\mathbf{u}}} \quad & ||\ddot{\mathbf{x}} - \ddot{\mathbf{x}}_{des}||^2_W \\ \text{s.t.} \quad & \widehat{\mathbf{M}}\ \ddot{\widehat{\mathbf{q}}} = \widehat{\mathbf{f}} + \widehat{\mathbf{u}} \\ & \ddot{\mathbf{x}} = \mathbf{J}\ddot{\mathbf{q}} + \dot{\mathbf{J}}\dot{\mathbf{q}} \\ & \widehat{\mathbf{u}}_l \leq \widehat{\mathbf{u}} \leq \widehat{\mathbf{u}}_u \end{aligned} \quad (16)$$

where $||\cdot||^2_W$ is the weighted 2-norm cost, $\mathbf{J}$ and $\dot{\mathbf{J}}$ are the task space Jacobian and its time derivative. $\widehat{\mathbf{u}}$ was obtained by solving the above constrained optimization problem at each timestep. Since the constraints are linear functions of

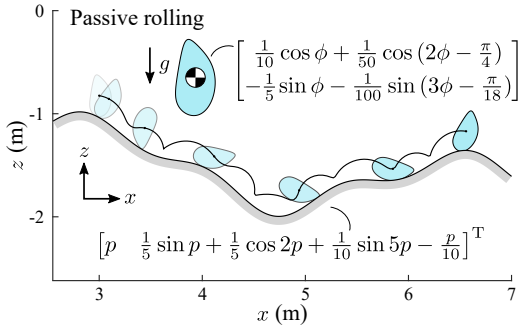

Fig. 6 **Passive rolling of an oblong rock on undulating terrain**. This simulation demonstrates that our formulation models dynamic rolling without slip for variable curvature body and terrain curves.

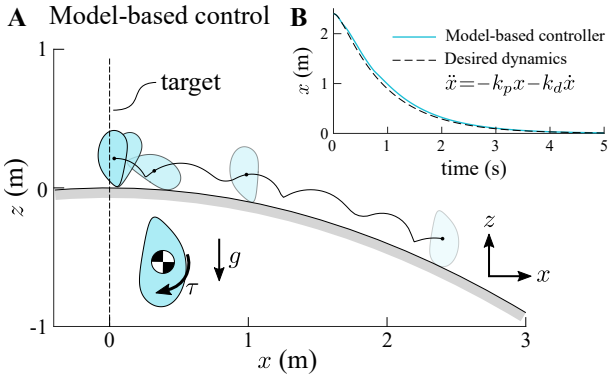

Fig. 7 **Stabilizing controller for an oblong rock. A.** A model-based Operational Space Controller (OSC) rolling an oblong rock up a parabolic hill. **B.** The OSC shows good convergence to the desired dynamics.

the decision variables, the problem can be solved as a convex quadratic program (QP) in real-time [48].

III. Results

We simulated several systems using our framework in MATLAB on a standard laptop computer. `ode23` was used to solve (15) and we solved for $\ddot{\mathbf{q}}$ using a least-squares solver. The supplementary material contains videos of our results (https://youtu.be/EtPQEzkqsK8) .

A. Simulation of a rock on undulating terrain

We simulated passive dynamic rolling of an oblong rock on undulating terrain (Fig. 6). The rock starts at rest at $x = 3$, gains velocity as it rolls downhill and slows down as it rolls uphill. Despite the constraints being enforced at the acceleration level, the position-level rolling constraints are closely enforced.

B. Model-based control of a rock on parabolic terrain

To demonstrate real-time control, we created a model-based controller to roll the oblong rock up a parabolic hill (Fig. 7A). The control input was an external torque. We used our model-based OSC to implement a simple feedback control law,

$$\ddot{\mathbf{x}}_{des} = k_p(0 - \mathbf{x}) + k_d(0 - \dot{\mathbf{x}}) \tag{17}$$

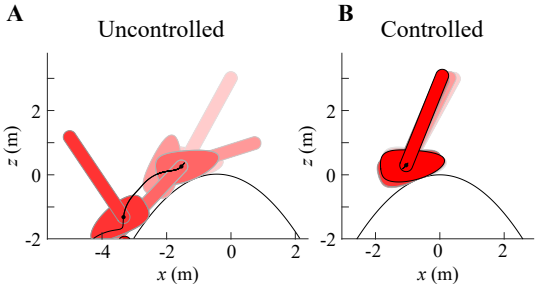

Fig. 8 **Dynamic balancing of an underactuated leg. A**. The uncontrolled system is highly unstable. **B**. The OSC applies a torque at the ankle and successfully balances the leg by achieving a multi-objective task.

where the gains k_p and k_d were chosen to be 10 and the task space $\mathbf{x}$ was the horizontal position of the body center. The OSC optimization (16) was solved as a convex quadratic program (QP) using MATLAB's `quadprog` interior point solver, which solved every QP in $<$ 3ms. The controller was implemented with a 100 Hz control rate in an `ode23` variable time-step simulation. Fig. 7A illustrates the model-based controller rolling the oblong rock up a parabolic hill towards the desired horizontal position of $\mathbf{x} = 0$ m. After 5 seconds, the rock's position converges to the desired position and comes to rest.

While many controllers could roll a rock, the OSC has some notable features. First, the horizontal position $\mathbf{x}$ does not noticeably accelerate or decelerate despite rapid changes in the vertical position (Fig. 7B). The controller is aware of the body and terrain curvature and adjusts its applied torques accordingly to achieve the desired acceleration, $\ddot{\mathbf{x}}$. Further, Fig. 7B shows the controller convergence rate is nearly identical to the desired linear dynamics (17), showing how accurately our modeling framework captures the curved rolling dynamics for real-time control.

C. Dynamic balancing of a 2-DoF leg on parabolic terrain

Balancing is an important objective in legged locomotion. We tested our framework on a planar underactuated leg on parabolic terrain. As seen in Fig. 8A, the uncontrolled system is highly unstable. The foot oscillates once near the terrain apex and rapidly rolls off backwards. In the controlled system (Fig. 8B), a torque is applied at the ankle joint. The task space is the shin angle in the global frame and the horizontal position of the ankle joint, and the two objectives are to hold the shin $\pi/10$ *rad* from the vertical and the ankle joint near the apex of the parabola. As the foot oscillates on the terrain, the OSC applies an ankle torque to adjust the shin angle and the foot position. Eventually the system settles into an oscillation near the apex. Note that there is an inherent tradeoff between the two objectives since the system has only one actuator. The controller successfully balances the leg despite this difficulty. This result shows that our formulation can be applied to underactuated multibody systems to perform challenging multi-objective tasks.

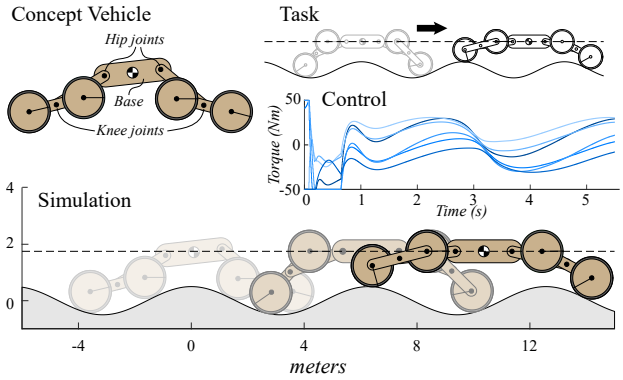

Fig. 9 **Wheel-leg UGV control on sinusoidal terrain.** The OSC successfully achieves the task despite large variations in joint accelerations produced by the variable curvature terrain.

D. Control of a wheel-leg UGV on sinusoidal terrain

In our previous work, we used motion planning to traverse a step obstacle with a wheel-leg Unmanned Ground Vehicle (UGV) [42]. In this work, we applied our auxiliary coordinate and OSC framework to control the UGV on sinusoidal terrain (Fig. 9). Each joint of the UGV is actuated, having a torque-controlled input at each hip, knee, and wheel. The tasks are to keep the base horizontal, maintain a constant base forward velocity, and constant base and non-rolling wheel heights. The controller converges to the desired set-points within 1 second. The variable terrain curvature produces large changes in joint accelerations as the rolling wheels asynchronously traverse the convex and concave terrain segments. The curvature-aware OSC maintains the desired behavior through these variations without relying on collision detection and contact force solvers. This result shows that our framework can achieve varied task-space objectives for locomotion on variable curvature terrain.

IV. Discussion

Our formulation can be employed for model-based real-time estimation, planning, and control over rough terrain. We had previously developed a motion planning framework for wheel-leg and track-leg UGVs with intermittent contact on piecewise linear terrain [42]. Variable curvature geometry can be particularly useful for modeling tracked systems. Using the techniques from our previous work, we also plan to include intermittent contact in our formulation.

Our rolling formulation has benefits over the classical zero-relative-velocity constraint [20]. On linear terrain, the tangent (and normal) direction at the contact point remains constant. When the tangent direction is constant, the contact point can be easily located; therefore the classical approach is suitable for linear terrain. However, for curved terrain, the tangent direction at the contact point varies as the body rolls (Fig. 2). In this case, collision detection is required to locate the contact point to apply the classical zero-relative-velocity constraint. In our formulation, collision detection is not required for the single-contact-point case. The contact point is located by solving for ϕ and p values that satisfy (13).

Our auxiliary formulation currently assumes a unique contact point. It cannot handle cases that result in multiple simultaneous contacts; such as a non-convex body rolling on linear terrain. Currently, this results in penetration at points distinct from the modeled contact point. We plan to address this in the future. Analytical solutions for collision detection are an active area of research [20], but iterative methods based on the common normal concept can also be used.

Currently, there are no bounds on the friction forces in the OSC. In the future, we plan to include friction cone constraints. Moreover, disturbances such as slip are important considerations in the real world. To compensate for such disturbances, we can use feedback control. Further, since the constraints are enforced at the acceleration level, they will eventually drift. We plan to use Baumgarte's stabilization method to address this [49].

V. Conclusion

Model-based real-time locomotion algorithms tend to overlook terrain curvature in their models. We developed a closed-form dynamic model that enables smooth planar parametric curves to roll without slipping. We achieved this by introducing auxiliary coordinates to define the parametric curves. We also developed an Operational Space Controller (OSC) for our rolling model. To verify our approach, we simulated an arbitrarily curved rock rolling on undulating terrain and generated control signals to stabilize it on parabolic terrain using the OSC. We also applied this framework to dynamically balance an underactuated 2-DoF leg on parabolic terrain and to control a wheel-leg UGV on sinusoidal terrain in simulation. Our formulation is suitable for real-time implementation as it solves in < 3 ms.

References

[1] "Curiosity Mars rover by NASA," https://mars.nasa.gov/msl/home/, accessed 2022 December 07.

[2] "Spirit and Opportunity Mars rovers by NASA," https://mars.nasa.gov/mer/, accessed 2022 December 07.

[3] M. Bjelonic, R. Grandia, O. Harley, C. Galliard, S. Zimmermann, and M. Hutter, "Whole-body MPC and online gait sequence generation for wheeled-legged robots," in *2021 IEEE/RSJ International Conference on Intelligent Robots and Systems (IROS)*. IEEE, 2021, pp. 8388–8395.

[4] A. Laurenzi, E. M. Hoffman, and N. G. Tsagarakis, "Quadrupedal walking motion and footstep placement through linear model predictive control," in *2018 IEEE/RSJ International Conference on Intelligent Robots and Systems (IROS)*. IEEE, 2018, pp. 2267–2273.

[5] W. Reid, F. J. Pérez-Grau, A. H. Göktoğan, and S. Sukkarieh, "Actively articulated suspension for a wheel-on-leg rover operating on a martian analog surface," in *2016 IEEE International Conference on Robotics and Automation (ICRA)*. IEEE, 2016, pp. 5596–5602.

[6] J. Sun, Y. You, X. Zhao, A. H. Adiwahono, and C. M. Chew, "Towards more possibilities: Motion planning and control for hybrid locomotion of wheeled-legged robots," *IEEE Robotics and Automation Letters*, vol. 5, no. 2, pp. 3723–3730, 2020.

[7] R. Tedrake, *Underactuated Robotics*, 2023. [Online]. Available: https://underactuated.csail.mit.edu

[8] R. M. Murray *et al.*, "Optimization-based control," *California Institute of Technology, CA*, pp. 111–128, 2009.

[9] A. E. Martin, D. C. Post, and J. P. Schmiedeler, "The effects of foot geometric properties on the gait of planar bipeds walking under hzd-based control," *The International Journal of Robotics Research*, vol. 33, no. 12, pp. 1530–1543, 2014.

[10] C. Chevallereau, G. Abba, F. Plestan, E. Westervelt, C. C. de Wit, J. Grizzle *et al.*, "Rabbit: A testbed for advanced control theory," *IEEE Control Systems Magazine*, vol. 23, no. 5, pp. 57–79, 2003.

[11] J. W. Grizzle, J. Hurst, B. Morris, H.-W. Park, and K. Sreenath, "Mabel, a new robotic bipedal walker and runner," in *2009 American Control Conference*. IEEE, 2009, pp. 2030–2036.

[12] M. Hutter, C. Gehring, D. Jud, A. Lauber, C. D. Bellicoso, V. Tsounis, J. Hwangbo, K. Bodie, P. Fankhauser, M. Bloesch *et al.*, "ANYmal-a highly mobile and dynamic quadrupedal robot," in *2016 IEEE/RSJ international conference on intelligent robots and systems (IROS)*. IEEE, 2016, pp. 38–44.

[13] A. E. Martin, D. C. Post, and J. P. Schmiedeler, "Design and experimental implementation of a hybrid zero dynamics-based controller for planar bipeds with curved feet," *The International Journal of Robotics Research*, vol. 33, no. 7, pp. 988–1005, 2014.

[14] P. A. Bhounsule, J. Cortell, A. Grewal, B. Hendriksen, J. D. Karssen, C. Paul, and A. Ruina, "Low-bandwidth reflex-based control for lower power walking: 65 km on a single battery charge," *The International Journal of Robotics Research*, vol. 33, no. 10, pp. 1305–1321, 2014.

[15] M. Cook, *Sleight of Mind: 75 Ingenious Paradoxes in Mathematics, Physics, and Philosophy*. MIT Press, 2020.

[16] J. Lawrence, *A Catalog of Special Plane Curves*, ser. Dover Books on Mathematics. Dover Publications, 2013.

[17] E. Lockwood, *A Book of Curves*. Cambridge University Press, 1967.

[18] D. Liberzon, *Calculus of variations and optimal control theory: a concise introduction*. Princeton university press, 2011.

[19] H. A. Rothbart, *Cam design handbook*. McGraw-Hill Education, 2004.

[20] U. J. Roemer, A. Fidlin, and W. Seemann, "Explicit analytical solutions for two-dimensional contact detection problems between almost arbitrary geometries and straight or circular counterparts," *Mechanism and Machine Theory*, vol. 128, pp. 205–224, OCT 2018.

[21] C. L. Collins, "Kinematics of robot fingers with circular rolling contact joints," *Journal of Robotic Systems*, vol. 20, no. 6, pp. 285–296, 2003.

[22] C. Cai and B. Roth, "On the spatial motion of a rigid body with line contact," in *Proceedings. 1988 IEEE International Conference on Robotics and Automation*, 1988, pp. 1036–1041 Vol.2.

[23] M. L. Turner, *Programming dexterous manipulation by demonstration*. Stanford University, 2001.

[24] L. Han and J. C. Trinkle, "Dextrous manipulation by rolling and finger gaiting," in *Proceedings. 1998 IEEE International Conference on Robotics and Automation (Cat. No. 98CH36146)*, vol. 1. IEEE, 1998, pp. 730–735.

[25] T. Pang, H. T. Suh, L. Yang, and R. Tedrake, "Global planning for contact-rich manipulation via local smoothing of quasi-dynamic contact models," *IEEE Transactions on Robotics*, 2023.

[26] J. Z. Woodruff and K. M. Lynch, "Robotic contact juggling," *IEEE Transactions on Robotics*, 2023.

[27] S. Andrews, K. Erleben, and Z. Ferguson, "Contact and friction simulation for computer graphics," in *ACM SIGGRAPH 2022 Courses*, 2022, pp. 1–172.

[28] D. E. Stewart, "Rigid-body dynamics with friction and impact," *SIAM review*, vol. 42, no. 1, pp. 3–39, 2000.

[29] E. Drumwright and J. C. Trinkle, *Contact Simulation*. Dordrecht: Springer Netherlands, 2019, pp. 1877–1931. [Online]. Available: https://doi.org/10.1007/978-94-007-6046-2_25

[30] S. Boyd, S. P. Boyd, and L. Vandenberghe, *Convex optimization*. Cambridge university press, 2004.

[31] M. Anitescu, "Optimization-based simulation of nonsmooth rigid multibody dynamics," *Mathematical Programming*, vol. 105, pp. 113–143, 2006.

[32] A. Tasora and M. Anitescu, "A complementarity-based rolling friction model for rigid contacts," *Meccanica*, vol. 48, pp. 1643–1659, 2013.

[33] R. W. Cottle, J.-S. Pang, and R. E. Stone, *The linear complementarity problem*. SIAM, 2009.

[34] A. Aydinoglu and M. Posa, "Real-time multi-contact model predictive control via ADMM," in *2022 International Conference on Robotics and Automation (ICRA)*. IEEE, 2022, pp. 3414–3421.

[35] M. Posa, C. Cantu, and R. Tedrake, "A direct method for trajectory optimization of rigid bodies through contact," *The International Journal of Robotics Research*, vol. 33, no. 1, pp. 69–81, 2014.

[36] P. G. Adamczyk, S. H. Collins, and A. D. Kuo, "The advantages of a rolling foot in human walking," *Journal of Experimental Biology*, vol. 209, no. 20, pp. 3953–3963, 2006.

[37] F. Asano and Z.-W. Luo, "On energy-efficient and high-speed dynamic biped locomotion with semicircular feet," in *2006 IEEE/RSJ International Conference on Intelligent Robots and Systems*. IEEE, 2006, pp. 5901–5906.

[38] T. Hase, Q. Huang, and X. Chen, "Performance analysis of biped walking robot with circular feet using optimal trajectory planning method," in *2008 IEEE International Conference on Robotics and Biomimetics*. IEEE, 2009, pp. 143–148.

[39] A. E. Martin, D. C. Post, and J. P. Schmiedeler, "Design and experimental implementation of a hybrid zero dynamics-based controller for planar bipeds with curved feet," *The International Journal of Robotics Research*, vol. 33, no. 7, pp. 988–1005, 2014.

[40] T. McGeer *et al.*, "Passive dynamic walking," *International Journal of Robotics Research*, vol. 9, no. 2, pp. 62–82, 1990.

[41] S. H. Collins, M. Wisse, and A. Ruina, "A three-dimensional passive-dynamic walking robot with two legs and knees," *The International Journal of Robotics Research*, vol. 20, no. 7, pp. 607–615, 2001.

[42] A. Mane, D. Swart, J. White, and C. Hubicki, "Trajectory optimization formulation with smooth analytical derivatives for track-leg and wheel-leg ground robots," in *2022 International Conference on Robotics and Automation (ICRA)*. IEEE, 2022, pp. 5762–5768.

[43] "Error found in SAT Question," *The New York Times*, p. 23, May 1982. [Online]. Available: https://www.nytimes.com/1982/05/25/us/error-found-in-sat-question.html

[44] A. Laulusa and O. A. Bauchau, "Review of classical approaches for constraint enforcement in multibody systems," *Journal of Computational and Nonlinear Dynamics*, vol. 3, no. 1, 2008.

[45] R. Murray, Z. Li, S. Sastry, and S. Sastry, *A Mathematical Introduction to Robotic Manipulation*. CRC Press, 1994.

[46] J. García de Jalón and M. D. Gutierrez-Lopez, "Multibody dynamics with redundant constraints and singular mass matrix: existence, uniqueness, and determination of solutions for accelerations and constraint forces," *Multibody System Dynamics*, vol. 30, pp. 311–341, 2013.

[47] T. Apgar, P. Clary, K. Green, A. Fern, and J. W. Hurst, "Fast online trajectory optimization for the bipedal robot cassie." in *Robotics: Science and Systems*, vol. 101. Pittsburgh, Pennsylvania, USA, 2018, p. 14.

[48] B. Stellato, G. Banjac, P. Goulart, A. Bemporad, and S. Boyd, "OSQP: An operator splitting solver for quadratic programs," *Mathematical Programming Computation*, vol. 12, no. 4, pp. 637–672, 2020.

[49] O. A. Bauchau and A. Laulusa, "Review of contemporary approaches for constraint enforcement in multibody systems," *Journal of Computational and Nonlinear Dynamics*, vol. 3, no. 1, 2008.